

Quantum Monte Carlo study of sodium

Ryo Maezono

*TCM Group, Cavendish Laboratory, University of Cambridge, Madingley Road, Cambridge CB3 0HE, United Kingdom
and National Institute for Materials Science, Computational Materials Science Center, Sengen 1-2-1,
Tsukuba, Ibaraki, 305-0047, Japan*

M. D. Towler, Y. Lee, and R. J. Needs

*TCM Group, Cavendish Laboratory, University of Cambridge, Madingley Road, Cambridge CB3 0HE, United Kingdom
(Received 19 May 2003; revised manuscript received 22 July 2003; published 14 October 2003)*

We report a variational and diffusion quantum Monte Carlo study of sodium. Pseudopotentials are used to represent the ion cores, and core-valence correlation effects are included by using a core polarization potential. When the core polarization potential is included we obtain an excellent value for the first ionization energy of the atom and a good value for the cohesive energy of the solid. Variational calculations of the occupied bandwidth give larger values than experiment, in agreement with recent sophisticated many-body calculations. Including the core polarization potential narrows the bandwidth slightly.

DOI: 10.1103/PhysRevB.68.165103

PACS number(s): 71.27.+a, 75.30.Et

I. INTRODUCTION

Variational and diffusion quantum Monte Carlo (VMC and DMC) methods have been used to study both insulating and metallic solids.¹ There have been rather few studies of metals other than the jellium model, probably because the finite size effects are larger in metals than in insulators. It is therefore of significance to establish the accuracy of the VMC and DMC methods for a real metal.

Here we report calculations of the ionization energy of the sodium atom and the cohesive energy, the occupied bandwidth and the pair correlation functions (PCFs) of solid sodium. It is often thought that the valence electrons in sodium metal are well represented by the jellium model, but in fact there are significant differences due to the lattice potential and the dynamical polarizability of the core electrons. Here we include the effects of the lattice potential via relativistic Hartree-Fock (HF) pseudopotentials, and the polarizability of the cores is described by a core polarization potential (CPP). To our knowledge, this work represents the first use of CPPs in quantum Monte Carlo (QMC) calculations for a periodic system.

The cohesive energy of sodium is well established experimentally, but the size of the occupied bandwidth of alkali metals, particularly sodium, has been the subject of much controversy. The discrepancy between the experimental values for the occupied bandwidth^{2,3} of 2.5–2.65 eV and the value of 3.6 eV obtained in recent sophisticated many-body perturbation theory calculations⁴ is remarkably large. In this paper we address the issues of the effects of the lattice potential, the polarizability of the core, and the electron-electron interaction on the bandwidth of sodium.

The plan of this paper is as follows. In Sec. II we describe the calculational methods, including the implementation of CPPs within periodic boundary conditions and the method for evaluating PCFs. In Sec. III we present and discuss the results for the atomic and solid energies, Sec. IV deals with the valence bandwidth, and Sec. V covers the PCF results. We draw our conclusions in Sec. VI.

II. DESCRIPTION OF THE CALCULATIONS**A. VMC and DMC methods**

In the VMC method the energy is calculated as the expectation value of the Hamiltonian with an approximate many-body trial wave function, the integrals being performed by a Monte Carlo method. The trial wave function normally contains a number of variable parameters, whose values are obtained by an optimization procedure.

The DMC approach is a stochastic method for evolving a wave function according to the imaginary-time Schrödinger equation.¹ Exact imaginary-time evolution would lead to the exact fermion ground state wave function, provided it has a nonzero overlap with the initial fermion state. However, the stochastic evolution is never exact and the solution converges to the bosonic ground state. In DMC calculations the fermionic symmetry is maintained by the fixed-node approximation,⁵ in which the nodal surface of the wave function is constrained to equal that of a guiding wave function. Typically the guiding wave function is taken to be the optimized trial wave function used in a VMC calculation. The fixed-node DMC energy provides a variational upper bound on the ground state energy with an error that is second order in the error in the nodal surface.^{6,7}

The fixed-node constraint also allows the study of excited states. The DMC algorithm converges to the lowest energy state consistent with the fixed nodal surface. If the fixed nodal surface is exactly that of an eigenstate the DMC algorithm gives the exact energy of that state. If we use a guiding wave function whose nodal surface approximates that of an excited state then the DMC energy will normally be a good approximation to the energy of the excited state. However, for excited states, the existence of a variational principle is dependent upon the symmetry of the guiding wave function.⁸

The trial and guiding wave functions introduce importance sampling and control both the statistical efficiency and the final accuracy that can be obtained. In the DMC method the final accuracy depends only on the nodal surface of the guiding wave function via the fixed-node approximation,

while in the VMC method the final accuracy depends on the entire trial wave function, so that VMC energies are more sensitive to the quality of the approximate wave function than DMC energies.

B. Trial/guiding wave functions

We have used trial and guiding wave functions of the standard Slater-Jastrow form,

$$\Psi(\mathbf{R}) = e^{J(\mathbf{R})} D_{\uparrow}(\mathbf{r}_1, \dots, \mathbf{r}_{N_{\uparrow}}) D_{\downarrow}(\mathbf{r}_{N_{\uparrow}+1}, \dots, \mathbf{r}_N), \quad (1)$$

where there are N electrons of which N_{\uparrow} are up-spin and $N - N_{\uparrow}$ are down-spin. $\mathbf{R} = (\mathbf{r}_1, \dots, \mathbf{r}_N)$ denotes the spatial coordinates of all the electrons, and $e^{J(\mathbf{R})}$ is the Jastrow correlation factor. The Slater determinants, D_{σ} , were formed from single-particle orbitals obtained from density functional theory calculations using the CRYSTAL98 Gaussian basis set code.⁹ For these calculations we used the Perdew-Burke-Ernzerhof [PBE] (Ref. 10) generalized gradient approximation for the exchange and correlation energy. Our Gaussian basis consisted of three uncontracted s functions with exponents 1.7974, 0.5676, and 0.053 a.u., and two uncontracted p functions with exponents 0.3795 and 0.0512 a.u. The Na^+ ions were described by relativistic Hartree-Fock pseudopotentials,¹¹ because they have been shown to give better results than density functional theory (DFT) ones when used within QMC calculations¹² and because CPPs are devised for use with Hartree-Fock pseudopotentials. The nonlocal pseudopotential energy was evaluated within the locality approximation.¹³ All of the QMC calculations were performed using the CASINO code.¹⁴

Jastrow factors take the form

$$J(\mathbf{R}) = - \sum_{i>j} \left\{ \frac{A}{r_{ij}} \left[1 - \exp\left(-\frac{r_{ij}}{F}\right) \right] \exp\left(-\frac{r_{ij}^2}{L_0^2}\right) + S_1(r_{ij}) \right\} - \sum_{i,I} S_2(r_{iI}), \quad (2)$$

where the indices i and j denote electrons and I denotes ions. F is chosen so that the cusp conditions¹⁵ are obeyed, i.e., $F_{\uparrow\uparrow} = \sqrt{2A}$ and $F_{\uparrow\downarrow} = \sqrt{A}$, and S_1 and S_2 are cusplless. We choose $L_0 = 0.3L_{\text{WS}}$, so that the first term in Eq. (2) is effectively zero at the shortest distance to the surface of the Wigner-Seitz cell, L_{WS} . S_1 and S_2 are expressed as polynomial expansions in the inter-particle distances. We used a total of 11 variable parameters in the Jastrow factor whose optimal values were obtained by minimizing the variance of the energy.^{16,17}

C. Simulation cells

At very low temperatures sodium crystallizes in a structure which consists of close-packed layers, probably in the $9R$ stacking,¹⁸ but at 35 K it undergoes a martensitic transition to the body-centered cubic (bcc) structure, which we study here. We use the experimental value of the cubic lattice constant of sodium at 78 K of $a = 4.235 \text{ \AA}$ (8.003 a.u.).¹⁹

QMC calculations for solids use finite simulation cells subject to periodic boundary conditions, which inevitably introduces finite size errors. We used the symmetric set of bcc primitive translation vectors $(\frac{1}{2}, \frac{1}{2}, -\frac{1}{2})a$, $(\frac{1}{2}, -\frac{1}{2}, \frac{1}{2})a$, and $(-\frac{1}{2}, \frac{1}{2}, \frac{1}{2})a$, and to form the different simulation cells we multiplied each of the primitive translation vectors by 2, 4, 6, 7, or 8, giving simulation cells containing 8, 64, 216, 343, and 512 atoms, respectively.

D. ‘‘Open shell’’ problem

In a metallic system at zero temperature the total number of orbitals below the Fermi should coincide with the number of electrons in the simulation cell. One would like to fill all degenerate orbitals, creating a ‘‘closed-shell’’ configuration, which guarantees that the charge density has the correct symmetry. However, in many cases the number of electrons and orbitals do not match and one has to use an ‘‘open shell’’ configuration. This problem is solved within mean-field calculations by using fractional occupations. In many-body calculations one could use a multi-determinant wave function to achieve a similar result, but this is inconvenient. Open shells can always be avoided in many-body calculations for the homogeneous electron gas (HEG) by filling complete shells and adjusting the size of the simulation cell to give the correct density. However, for a real metal there is less freedom to adjust the cell size as it must consist of an integer number of primitive cells, and if a single determinant is to be used one may be forced to use an open shell configuration.

DMC calculations require the use of real wave functions. We construct these by forming real orbitals from the degenerate complex Bloch orbitals as $\phi_+ = (1/\sqrt{2})[\phi_{\mathbf{k}} + \phi_{\mathbf{k}}^*]$ and $\phi_- = (1/i\sqrt{2})[\phi_{\mathbf{k}} - \phi_{\mathbf{k}}^*]$, as described in Appendix A. The up- and down-spin determinants can be partitioned into closed and open shell parts. The closed shell parts can be written in terms of the real orbitals, ϕ_+ and ϕ_- , as the Bloch orbitals at \mathbf{k} and $-\mathbf{k}$ are both occupied. For the open shell parts we simply use the appropriate number of the ϕ_+ and ϕ_- orbitals. For the largest cell containing 512 electrons it is not possible to choose a closed shell configuration, and there are two holes in the outermost shell. We choose these holes to be of opposite spin and include the required number of ϕ_+ and ϕ_- orbitals. When there is only a single hole of each spin type the HF energy expectation value can be shown to be independent of which orbitals are selected, even though the charge density may depend on the selection. In QMC calculations the energy can depend on the selection of orbitals but we expect this effect to be small.

Recent QMC tests of open shell configurations of solid aluminum at fixed system size²⁰ found energy differences between different fillings of the states of less than 0.1 eV per atom. A study as a function of system size indicated reasonable convergence after correction for finite size effects, but the range of system sizes studied was insufficient to draw firm conclusions on this point.

E. Core polarization potential

It is consistent to use CPPs with HF pseudopotentials to account for the core-valence correlation effects and the static

polarization effects due to the other ions in the system. As, to our knowledge, this paper reports the first use of CPPs in QMC calculations for extended systems we devote some space to describing our implementation for systems with periodic boundary conditions.

In the CPP approximation the polarization of a particular core is determined by the electric field at the nucleus. The electric field acting on the ion core at \mathbf{R}_I due to the other ions at \mathbf{R}_J and the electrons at \mathbf{r}_i is²¹

$$\mathbf{F}_I = - \sum_{J \neq I} \frac{\mathbf{R}_{JI}}{R_{JI}^3} Z_J + \sum_i \frac{\mathbf{r}_{iI}}{r_{iI}^3}, \quad (3)$$

where $\mathbf{R}_{JI} = \mathbf{R}_J - \mathbf{R}_I$, $\mathbf{r}_{iI} = \mathbf{r}_i - \mathbf{R}_I$ and Z_J is the charge of ion J . The CPP energy operator is then

$$V_{\text{CPP}} = - \frac{1}{2} \sum_I \alpha_I |\mathbf{F}_I|^2, \quad (4)$$

where α_I is the dipole polarizability of core I .

Equation (3) assumes a classical description which is valid when the valence electrons are far from the cores and the cores are far from each another. When a valence electron penetrates the core the classical result is a very poor approximation, diverging at the nucleus. To remove this unphysical behavior each contribution to the electric field in Eq. (3) is multiplied by a cutoff function $f(r_{iI}/\bar{r}_I)$, where \bar{r}_I is a parameter, which tends to unity at large r_{iI} . A further possible modification is to allow the one-electron term in Eq. (4), which takes the form $-\alpha_I/(2r_{iI}^4)$, to depend on the angular momentum component, l , and replace the factor \bar{r}_I in the cutoff function by an angular momentum dependent parameter, \bar{r}_{Il} . With these modifications the CPP energy operator becomes

$$\begin{aligned} V_{\text{CPP}} = & - \frac{1}{2} \sum_I \alpha_I \left[\sum_i \frac{1}{r_{iI}^4} \sum_l f\left(\frac{r_{iI}}{\bar{r}_{Il}}\right)^2 \hat{P}_l \right. \\ & + \sum_i \sum_{j \neq i} \frac{\mathbf{r}_{iI} \cdot \mathbf{r}_{jI}}{r_{iI}^3 r_{jI}^3} f\left(\frac{r_{iI}}{\bar{r}_{Il}}\right) f\left(\frac{r_{jI}}{\bar{r}_{Ij}}\right) \\ & \left. - 2 \sum_i \sum_{J \neq I} \frac{\mathbf{r}_{iI} \cdot \mathbf{R}_{JI}}{r_{iI}^3 R_{JI}^3} f\left(\frac{r_{iI}}{\bar{r}_{Il}}\right) Z_J + \left(\sum_{J \neq I} \frac{\mathbf{R}_{JI}}{R_{JI}^3} Z_J \right)^2 \right], \end{aligned} \quad (5)$$

where \hat{P}_l is the projector onto the l th angular momentum component of the i th electron with respect to the I th ion.

For efficient evaluation we rewrite Eq. (5) as

$$\begin{aligned} V_{\text{CPP}} = & - \frac{1}{2} \sum_I \alpha_I |\bar{\mathbf{F}}_I|^2 + \frac{1}{2} \sum_I \alpha_I \sum_i \frac{1}{r_{iI}^4} \\ & \times \sum_{l=0}^{l_{\text{max}}} \left[f\left(\frac{r_{iI}}{\bar{r}_{Il}}\right)^2 - f\left(\frac{r_{iI}}{\bar{r}_{Ii}}\right)^2 \right] \hat{P}_l, \end{aligned} \quad (6)$$

where

$$\bar{\mathbf{F}}_I = - \sum_{J \neq I} \frac{\mathbf{R}_{JI}}{R_{JI}^3} Z_J + \sum_i \frac{\mathbf{r}_{iI}}{r_{iI}^3} f\left(\frac{r_{iI}}{\bar{r}_I}\right), \quad (7)$$

and $l_{\text{max}}=2$ is the maximum angular momentum. If there are N electrons and ions then direct evaluation of Eq. (5) requires $\mathcal{O}(N^3)$ operations while Eq. (6) can be evaluated in $\mathcal{O}(N^2)$ operations, which is the same order as for the other interaction terms.

We use the cutoff function^{22,23}

$$f(x) = (1 - e^{-x^2})^2. \quad (8)$$

For sodium only the s and p channels are significant and, for simplicity, in these calculations we have chosen to set $\bar{r}_{0I} = \bar{r}_{1I} = \bar{r}_{2I} = \bar{r}_I = 1.0307$ a.u., which is the radius for the s channel given by Shirley and Martin,²³ and we used $\alpha_I = 0.9776$ a.u., as given in the same paper. When only a single CPP radius is used the second term in Eq. (6) is zero. For periodic systems the electric fields $\bar{\mathbf{F}}_I$ are evaluated directly from the analytic first derivatives of the Ewald potential. The additional computational cost of calculating the CPP energy is small because many of the quantities involved must also be evaluated for the electron-electron and electron-ion interaction energies.

F. Model periodic Coulomb interaction

The model periodic Coulomb (MPC) interaction^{24–26} was introduced into QMC calculations within periodic boundary conditions to reduce finite size effects arising from the use of the Ewald interaction to model the Coulomb interaction. The interaction energy can be divided into Hartree and exchange-correlation terms. The basic idea^{24–26} of the MPC interaction is that the Ewald interaction introduces an error because the interaction of an electron with its exchange-correlation hole is not $1/r$, as it would be in an infinite system. In the MPC formulation each electron interacts with its exchange-correlation hole via the $1/r$ Coulomb potential, while the Hartree energy is evaluated using the Ewald interaction. In this study we use the MPC and Ewald interactions to test whether the Coulomb finite size effects are significant. When the difference between the energies calculated with the MPC and Ewald interactions is negligible we assume that the simulation cell is sufficiently large that the Coulomb finite size effects are negligible. Our implementation of the MPC interaction, which has not been described in the literature before, is summarized in Appendix B.

G. Pair correlation functions

The PCF can be written as

$$g(\mathbf{x}, \mathbf{x}') = \frac{\rho(\mathbf{x}, \mathbf{x}')}{n(\mathbf{x})n(\mathbf{x}')}, \quad (9)$$

where \mathbf{x} denotes the spatial and spin components. For N electrons ρ is

$$\rho(\mathbf{x}, \mathbf{x}') = N(N-1) \frac{\int |\Psi(\mathbf{x}_1, \mathbf{x}_2, \dots, \mathbf{x}_N)|^2 \delta(\mathbf{x} - \mathbf{x}_1) \delta(\mathbf{x}' - \mathbf{x}_2) d\mathbf{x}_1, \dots, d\mathbf{x}_N}{\int |\Psi(\mathbf{x}_1, \mathbf{x}_2, \dots, \mathbf{x}_N)|^2 d\mathbf{x}_1, \dots, d\mathbf{x}_N}. \quad (10)$$

Calculating the full six-dimensional function $\rho(\mathbf{x}, \mathbf{x}')$ is very costly, although it has been done within VMC calculations.^{27,28} It is less costly to calculate the PCF with one of the electron coordinates fixed at some chosen point. Fixing the position of a spin-up electron at \mathbf{r}_{fix} , the PCF can be written as

$$g_{\sigma\uparrow}(\mathbf{r}, \mathbf{r}_{\text{fix}}) = \frac{\rho_{\sigma\uparrow}(\mathbf{r}, \mathbf{r}_{\text{fix}})}{n_{\sigma}(\mathbf{r})n_{\uparrow}(\mathbf{r}_{\text{fix}})} = \frac{n_{\sigma}(\mathbf{r}; \mathbf{r}_{\text{fix}}, N_{\sigma} - \delta_{\sigma\uparrow})}{n_{\sigma}(\mathbf{r})}, \quad (11)$$

where $n_{\sigma}(\mathbf{r}; \mathbf{r}_{\text{fix}}, N_{\sigma} - \delta_{\sigma\uparrow})$ is the charge density of the $N_{\sigma} - \delta_{\sigma\uparrow}$ spin- σ electrons whose positions are not fixed, calculated with a spin-up electron fixed at \mathbf{r}_{fix} . The calculation of the PCF can therefore be reduced to evaluating the charge densities with and without fixing the position of an electron. This algorithm gives the correct PCF within both VMC and DMC approaches.

We have calculated the parallel and anti-parallel spin PCFs for sodium with the electron fixed half-way between two nearest neighbor atoms. The PCFs were accumulated in reciprocal space. These calculations give a good description of the overall shape of the PCFs, and show that they are almost spherically symmetric for $|\mathbf{r} - \mathbf{r}_{\text{fix}}| < \sim 8$ a.u., but the statistical noise makes detailed studies extremely costly. We therefore decided to study the spherical averages of the PCFs about the point \mathbf{r}_{fix} . The PCF of Eq. (11) can be written in spherical polar coordinates,

$$g_{\sigma\uparrow}(\mathbf{r}, \mathbf{r}_{\text{fix}}) = g_{\sigma\uparrow}(R, \theta, \phi), \quad (12)$$

where $R = |\mathbf{r} - \mathbf{r}_{\text{fix}}|$. The spherical average about \mathbf{r}_{fix} is then

$$\begin{aligned} \bar{g}_{\sigma\uparrow}(R, \mathbf{r}_{\text{fix}}) &= \frac{1}{4\pi} \int g_{\sigma\uparrow}(R, \theta, \phi) d\Omega \\ &= \frac{1}{4\pi R^2} \left\langle \sum_{j=1}^{N_{\sigma} - \delta_{\sigma\uparrow}} \frac{\delta(R - |\mathbf{r}_j - \mathbf{r}_{\text{fix}}|)}{n_{\sigma}(\mathbf{r}_j)} \right\rangle. \end{aligned} \quad (13)$$

Note the appearance of the weighting function $1/n_{\sigma}(\mathbf{r}_j)$ in Eq. (13). The parallel and anti-parallel spin PCFs were accumulated in real space by collecting in radial bins of width $\Delta r = 0.56$ a.u.

III. ENERGIES OF THE ATOM AND SOLID

As the pseudoatom contains only a single s electron its energy can be calculated by a numerical integration on a radial grid, which gave an ionization energy of 4.972 eV without the CPP and 5.149 eV including the CPP. As a simple check we also calculated the atomic energies within VMC and DMC approaches using the orbital from the numerical integration as the trial/guiding wave function, which

gave energies within error bars of the numerical integration values. Our value of the additional binding energy arising from the CPP of 0.177 eV is in excellent agreement with the value of 0.17 eV given in Ref. 23, and our ionization energy including the CPP is in excellent agreement with the experimental value of 5.14 eV.²⁹

We calculated the energies for the solid using 8-, 64-, 216-, and 512-atom simulation cells, using both the Ewald and MPC interactions and the VMC and DMC methods, both with and without the CPP. The fraction of the total correlation energy described by the Jastrow function can be measured by the quantity

$$Q = \frac{E_{\text{VMC}}^{\text{Slater-J}} - E_{\text{VMC}}^{\text{Slater}}}{E_{\text{VMC}}^{\text{Slater}} - E_{\text{DMC}}}, \quad (14)$$

where $E_{\text{VMC}}^{\text{Slater-J}}$ and $E_{\text{VMC}}^{\text{Slater}}$ denote the VMC energies with and without the Jastrow function, respectively. We found that Q slowly increased with system size, from 72(1)% for eight atoms to 90.5(4)% with 64 atoms to 93.4(5)% (216 atoms) and finally to 93.8(3)% for our largest cell containing 512 atoms. This indicates that the quality of our Jastrow factors slowly increases with system size although no discernible improvement is obtained beyond 216 atoms. This behavior is at least partly due to our procedure of cutting off the Jastrow factor smoothly at the shortest distance to the surface of the Wigner-Seitz cell [see Eq. (2)].

Figure 1 shows the system size dependence of the VMC and DMC ground state energies calculated using both the MPC and Ewald interactions, with and without the CPP, plotted as a function of $1/N$, where N is the number of atoms in

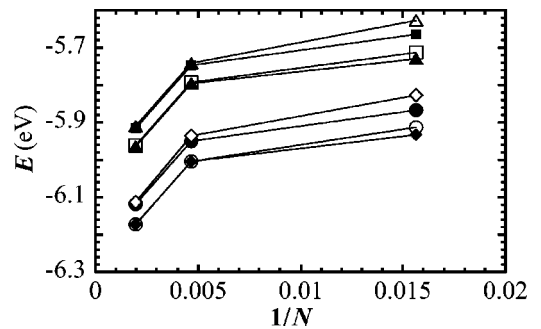


FIG. 1. VMC and DMC energies (eV per atom) as a function of $1/N$, where N is the number of atoms in the simulation cell. Open symbols denote results obtained with the MPC interaction and filled symbols denote those obtained with the Ewald interaction. Results with the CPP are denoted by circles and diamonds and those without the CPP are denoted by triangles and squares. DMC results are denoted by filled triangles, open circles, open squares, and filled diamonds, while the other symbols denote VMC results.

TABLE I. The DMC energies obtained using the Ewald interaction, with and without the CPP, and the PBE k -point correction $\Delta E_{PBE} = E_{PBE}(\infty) - E_{PBE}(N)$, as a function of the number of atoms in the simulation cell, N . All energies are in eV per atom.

N	DMC energy (with CPP)	DMC energy (no CPP)	ΔE_{PBE}
8	-5.51(3)	-5.465(2)	-0.923
64	-6.160(1)	-5.958(3)	0.228
216	-6.2042(7)	-5.9944(8)	0.201
512	-6.2319(3)	-6.0241(5)	0.061

the simulation cell. We incorporated k -point corrections obtained by taking the difference between PBE energies calculated for the actual simulation cells and for extremely large cells. These are essentially corrections for the kinetic energy. The numerical values of the uncorrected DMC energies, with and without the CPP, and the k -point corrections, are given in Table I. The very close agreement between the Ewald and MPC energies for the 216- and 512-atom systems shows that the Coulomb finite size effects are small for these system sizes. The energies calculated using the CPP are about 0.20(1) eV per atom lower than the corresponding energies calculated without the CPP, which is a slightly larger energy reduction than in the atom.

The VMC and DMC energy curves in Fig. 1 have very similar shapes, indicating that the source of the finite size errors is the same in each case. The finite size errors must therefore arise from the determinants used in the trial wave functions. These effects are reduced by the k -point corrections but clearly a significant error remains, which might be due to effects from the open shell configurations. We have tried to extrapolate the energies in Fig. 1 to an infinite system size, and although this results in improved values of the cohesive energy we are not convinced that the extrapolations are justified. We have therefore chosen to report our best results for the QMC solid energies as those for the largest system size studied of 512 atoms.

To obtain our final estimates of the solid energies we corrected them for the zero-point vibrational energy of the ions. The zero-point vibrational energy, E_{ZPE} was estimated using the standard Debye formula, $E_{ZPE} = 9k_B T_D / 8$, where T_D is the Debye temperature. Using $T_D = 150$ K (Ref. 30) gives $E_{ZPE} = 0.0145$ eV per atom.

The final cohesive energies together with the experimental value and some DFT values are given in Table II. Our best

TABLE II. Data for the cohesive energy of sodium. All values contain a correction for the zero-point energy of the solid of $E_{ZPE} = 0.0145$ eV per atom.

Cohesive energy (eV)	Source
1.13	Experiment (Ref. 32)
0.9437(8)	VMC without CPP
0.9694(8)	VMC with CPP
0.9910(5)	DMC without CPP
1.0221(3)	DMC with CPP
1.20	LDA
1.04	PBE
0.72	BLYP

QMC result is the DMC calculation with the CPP, which gives a cohesive energy in good agreement with experiment. The VMC cohesive energies are slightly smaller than the DMC ones. This is expected because the VMC and DMC atomic energies are essentially equal and exact, while the DMC solid energy is lower than the VMC solid energy because the DMC energy corresponds to calculating the energy with the exact Jastrow factor (but an approximate nodal surface). In Table II we also report all-electron results for the cohesive energy of sodium calculated within the local density approximation (LDA) and the PBE and Becke-Lee-Yang-Parr (BLYP) generalized gradient correction schemes. We believe that it is reasonable to compare with all-electron DFT results because our QMC calculations with CPPs include core-valence correlation effects. Our DFT cohesive energies are in good agreement with those of the recent study by Jaffe *et al.*³¹ The LDA slightly overestimates the cohesive energy, while the PBE slightly underestimates it. The cohesive energy obtained with BLYP is, on the other hand, much too small.

The comparison between the atomic and solid energies is nicely illustrated by Fig. 2. To construct this figure we have taken the zero of energy to be that of a Na^+ ion with its electron very far away, which is precisely the zero of energy for a pseudopotential calculation of a sodium atom. With this choice of zero the energy of the neutral sodium atom is equal to the negative of the ionization energy, while the energy of the solid is lower still by the cohesive energy. Figure 2 shows that the LDA, PBE, and BLYP density functionals give very similar values for the atomic ionization energy, which are somewhat larger than the experimental value. The LDA and PBE density functionals yield quite good cohesive energies,

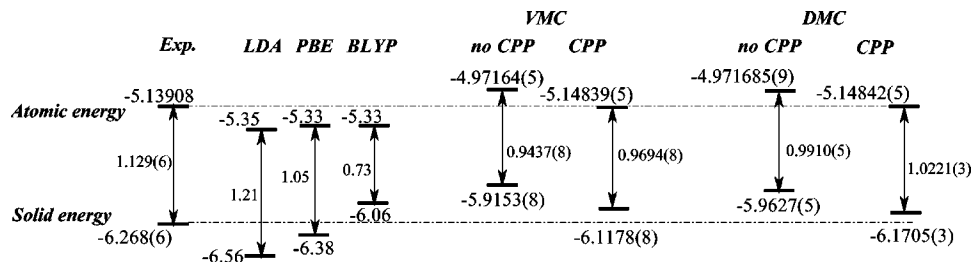


FIG. 2. Energies of the sodium atom and solid given in eV per atom from various calculations and from experiment. The zero of energy is that of a Na^+ ion with its electron very far away. The horizontal dash-dotted lines represent the experimental values deduced from the measured first ionization energy and the cohesive energy.

but the BLYP cohesive energy is much too small. The fairly accurate cohesive energies obtained in the LDA and PBE arise from a cancellation of the errors in the descriptions of the attraction of the valence electron to the core in the atom and solid. The LDA, PBE, and BLYP schemes are therefore not expected to give accurate energy differences between systems in which the charge on the sodium ions is different, and BLYP does not even give an accurate energy difference between the neutral atom and solid. The DMC method including the CPP, on the other hand, gives highly accurate values for the ionization energy and electron affinity,²³ a good value for the cohesive energy, and an equally good value for the binding energy of the sodium dimer.³³

IV. BANDWIDTH

We have calculated the occupied bandwidth within the QMC approach as the difference in energy between removing an electron from the lowest energy single-particle orbital at the Γ point and removing an electron from the highest energy occupied single-particle orbital. For each calculation we used the Jastrow factor optimized for the ground state. A much smaller error bar in the energy per atom is required for calculating the bandwidth than for the cohesive energy because the bandwidth is the difference between two energies for the entire simulation cell whereas the cohesive energy is the difference in energies per atom. For this reason we have not been able to perform DMC bandwidth calculations for the larger system sizes. Instead we have performed VMC bandwidth calculations for systems with up to 512 atoms and DMC calculations for systems with up to 216 atoms. For each system size we have added a finite-size correction calculated as the difference between the LDA bandwidth for the k -point grid used in the QMC calculation and the LDA bandwidth calculated with a large grid corresponding to a simulation cell containing 15 625 atoms, for which the finite size error in the LDA bandwidth is estimated to be less than 0.01 eV. The sizes of the k -point corrections vary from 0.64 eV

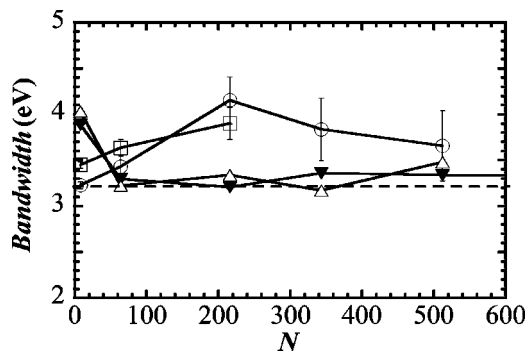


FIG. 3. The occupied bandwidth of sodium in eV calculated within VMC (open circles) and DMC (open squares) methods and using the LDA (filled triangles) and the PBE (open triangles). The error bars indicate the standard deviations in the means. The free electron bandwidth at the same average density of $r_s=3.94$ is shown as a horizontal dashed line. The k -point correction has been added to the VMC and DMC results, but not to the LDA or PBE results.

TABLE III. Data for the occupied bandwidth of sodium and for jellium at the same average density of $r_s=3.94$, and at $r_s=4$.

Bandwidth (eV)	Method
$2.5^2-2.65^3$	Experiment
3.7 ± 0.4	VMC, present work
3.25	LDA, present work
3.23	Free electron ($r_s=3.94$)
3.13	Free electron ($r_s=4$)
3.6^4	<i>GI</i> (jellium $r_s=4$)

for the eight-atom cell down to 0.09 eV for the 512-atom cell.

Various data for the occupied bandwidth of sodium and for jellium at densities of $r_s=3.94$ are given in Table III. By comparing the LDA bandwidth with the free electron bandwidth at the same density ($r_s=3.94$) we deduce that the lattice potential leads to a very small increase in the bandwidth of about 0.02 eV. We also found that the CPP gives only a very small change in the bandwidth, and therefore we calculated this change using a correlated sampling approach within the VMC approach. For all system sizes the CPP reduced the bandwidth, but only by 0.01–0.05 eV. Figure 3 shows the occupied VMC, DMC, LDA, and PBE bandwidths of sodium as a function of the size of the simulation cell. The DMC results for small system sizes are in reasonable agreement with the VMC results. Our VMC calculations show a broadening of the bandwidth for all system sizes studied (up to 512 electrons). Our best estimate of the QMC bandwidth was obtained from VMC calculations on the 512-electron simulation cell.

The bandwidth of sodium obtained from photoemission experiments^{2,3} is 2.5–2.65 eV, which is significantly narrower than the free electron bandwidth of 3.23 eV at the same average valence charge density. This band narrowing has been attributed to electron-electron interaction effects. Recently there has been renewed interest in this problem because new and more sophisticated many-body calculations have suggested that the effect of the electron-electron interactions may be to broaden the bandwidth. In their calculations using the *GI* method Yasuhara *et al.*⁴ obtained a bandwidth of about 3.6 eV, which is similar to the result obtained in more recent calculations by Takada^{34,35} using a similar approach.

The effect of the electron-electron interaction on the occupied bandwidth of the HEG results from a delicate competition between exchange and correlation effects. Within HF theory, the occupied bandwidth of the HEG at a density of $r_s \approx 4$ is about 4 eV larger than the free electron value, but electron correlation reduces the bandwidth to a value much closer to the free electron bandwidth. Because of the large cancellation between the exchange and correlation terms the need for a sophisticated treatment of electron-electron interactions for the bandwidth problem is clear.

According to Yasuhara *et al.*⁴ the conflict between their theoretical bandwidth of 3.6 eV and the experimental values of 2.5–2.65 eV might be resolved by invoking the effects of the electron-electron interaction on the final states in the pho-

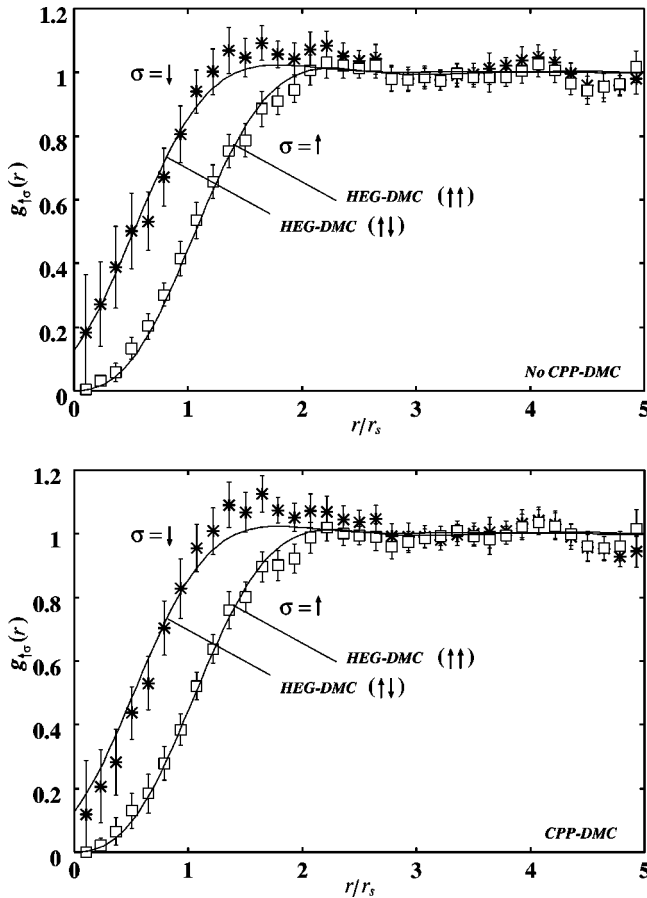


FIG. 4. Spherically averaged pair correlation function with an electron fixed halfway between two nearest neighbor atoms. The solid lines represent DMC results for the HEG at the same average density.

toemission process, although this suggestion has been strongly criticized.³⁶ Our VMC calculations give a bandwidth consistent with that of Yasuhara *et al.*⁴ However, QMC calculations of the bandwidths of silicon³⁷ and diamond³⁸ have given bandwidths larger than experiment. This overestimation of the bandwidth presumably results from the quality of the nodal surface of the state at the bottom of the band being poorer than for the state at the top of the band.

V. PAIR CORRELATION FUNCTIONS

Since the PCFs are local quantities they may be described accurately using fairly small simulation cells. We have used a simulation cell containing 64 atoms which adopts a closed shell electronic configuration, and consequently the trial wave function has the proper symmetry. We fixed a spin-up electron halfway between two nearest neighbor atoms, i.e., $\mathbf{r}_{\text{fix}} = (a/4, a/4, a/4)$. DMC results for the spherically averaged parallel and antiparallel PCFs are shown in Fig. 4, both with and without the CPP. For comparison, DMC results for the HEG (Ref. 39) at the same average density are shown as solid lines.

The PCFs for sodium have a little more structure than the HEG ones, but the extent of the exchange and correlation

holes is very similar. The parallel-spin PCF is hardly affected by the presence of the CPP but the anti-parallel-spin PCF is reduced for very small r and slightly increased around the first peak at about $r = 1.5r_s$. It turns out that the presence of the CPP increases the expectation value of the direct valence electron-electron interaction energy, both overall and when an electron is fixed at \mathbf{r}_{fix} . The expectation value of the CPP is, however, strongly negative, so that overall the CPP lowers the total energy. Note that the CPP affects the correlations between all the electrons, and one cannot expect the shapes of the PCFs plotted in Fig. 4 necessarily to reflect the overall changes in interaction energies due to the CPP.

VI. CONCLUSION

We have applied the VMC and DMC methods to sodium. The introduction of core-valence correlation via a CPP increases the binding of electrons to the atomic cores, resulting in excellent values for the atomic ionization energy. Using the DMC method and the CPP we obtain a good value for the cohesive energy of the solid, which has a similar level of accuracy to that obtained with the LDA and PBE density functional methods. The effect of the CPP largely cancels in the QMC cohesive energies. Sodium may be a difficult case for calculating the cohesive energy using the DMC method, because there is no fixed-node error in the pseudoatomic energy, so that the use of the fixed-node approximation always serves to reduce the cohesive energy. It is also clear from our results that significant finite size errors are present even for quite large system sizes, which may be due to the effects of the open shell configurations.

The LDA, PBE, and BLYP schemes make significant errors in the descriptions of the attraction of the valence electrons to the cores. These errors largely cancel in the cohesive energy within the LDA and PBE schemes, but in the BLYP scheme the cohesive energy is far too small. These results show the importance of using an accurate description of exchange and correlation in sodium.

Including the CPP narrows the occupied bandwidth slightly and has discernible effects upon the antiparallel spin PCF in the solid. The CPP may be important for other properties, and there are other situations in which incorporating CPPs leads to substantial improvements. Our VMC value for the occupied bandwidth of sodium of 3.7 ± 0.4 eV is significantly larger than the experimental value of 2.5–2.65 eV, but is in good agreement with a recent many-body calculation⁴ which used a sophisticated approximation for the electron self-energy. However, DMC calculations for silicon³⁷ and diamond³⁸ gave occupied bandwidths which are too large, and we suspect that the same may apply to our sodium calculations. A widely accepted solution to the bandwidth problem has not so far emerged. On the other hand, we believe that our conclusions that the effects of the static lattice potential and the dynamical core polarizability on the occupied bandwidth are very small are reliable.

ACKNOWLEDGMENTS

We thank Martin Vogt for useful conversations. Financial support was provided by Engineering and Physical Sci-

ences Research Council (EPSRC) of the United Kingdom. Our calculations were performed using the facilities of the Supercomputer Center (ISSP; Institute for Solid State Physics, University of Tokyo), the Center for Information Science of JAIST (Japan Advanced Institute of Science and Technology), the Computer Services for Academic Research (CSAR, University of Manchester), and the Cambridge-Cranfield High Performance Computing Facilities (HPCF). The authors would like to thank Professor Teruo Matsuzawa (JAIST) for the generous provision of computing facilities. R.M. would like to thank NIMS (National Institute for Materials Science) directors, Professor Teruo Kishi, Dr. Takehiko Matsumoto, and Dr. Taizo Sasaki for their special treatment during the overseas collaboration with the University of Cambridge.

APPENDIX A: CONSTRUCTING REAL ORBITALS

We use many-body Bloch wave functions constructed from the lowest energy single-particle orbitals calculated on a grid of k points,

$$\mathbf{k}_{lmn} = \frac{l}{q_1} \mathbf{b}_1 + \frac{m}{q_2} \mathbf{b}_2 + \frac{n}{q_3} \mathbf{b}_3 + \mathbf{k}_s, \quad (\text{A1})$$

where the q_i are integers, the \mathbf{b}_i are the primitive reciprocal lattice vectors, and $(0 \leq l \leq q_1 - 1)$, $(0 \leq m \leq q_2 - 1)$, and $(0 \leq n \leq q_3 - 1)$. In this study the offset vector, \mathbf{k}_s , was set to zero.

The Bloch orbitals at an arbitrary point in k -space are complex. If the set of wave vectors consists of $\pm \mathbf{k}$ pairs one can always construct a set of real orbitals spanning the same space as the original complex set. A necessary and sufficient condition for the grid of Eq. (A1) to consist of $\pm \mathbf{k}$ pairs is that $\mathbf{k}_s = \mathbf{G}_s/2$, where \mathbf{G}_s is a reciprocal lattice vector of the simulation cell lattice. If $\phi_{\mathbf{k}}$ is a Bloch function of wave vector \mathbf{k} then $\phi_{\mathbf{k}}^*$ is a Bloch function of wave vector $-\mathbf{k}$. Therefore we can make two real orbitals from $\phi_{\mathbf{k}}$ and $\phi_{\mathbf{k}}^*$ as follows:

$$\begin{aligned} \phi_+(\mathbf{r}) &= \frac{1}{\sqrt{2}} [\phi_{\mathbf{k}}(\mathbf{r}) + \phi_{\mathbf{k}}^*(\mathbf{r})], \\ \phi_-(\mathbf{r}) &= \frac{1}{i\sqrt{2}} [\phi_{\mathbf{k}}(\mathbf{r}) - \phi_{\mathbf{k}}^*(\mathbf{r})]. \end{aligned} \quad (\text{A2})$$

The orbitals ϕ_+ and ϕ_- are orthogonal if $\phi_{\mathbf{k}}$ and $\phi_{\mathbf{k}}^* = \phi_{-\mathbf{k}}$ are orthogonal, which holds unless $\mathbf{k} - (-\mathbf{k}) = \mathbf{G}_p$, where \mathbf{G}_p is a reciprocal lattice vector of the primitive lattice. In this case ϕ_+ and ϕ_- are linearly dependent and we must use only one of them, or one of ϕ_+ and ϕ_- must be zero, in which case we must obviously use the nonzero one. The scheme is therefore

$$\text{Case (1) if } \mathbf{k} \neq \frac{\mathbf{G}_p}{2} \text{ use } \phi_+ \text{ and } \phi_-,$$

$$\text{Case (2) if } \mathbf{k} = \frac{\mathbf{G}_p}{2} \text{ use } \phi_+ \text{ or } \phi_-. \quad (\text{A3})$$

APPENDIX B: MPC INTERACTION

The exact MPC interaction operator is^{25,26}

$$\begin{aligned} \hat{H}_{e-e}^{\text{exact}} &= \sum_{i>j} f(\mathbf{r}_i - \mathbf{r}_j) + \sum_i \int_{\text{WS}} n(\mathbf{r}) \\ &\quad \times [v_E(\mathbf{r}_i - \mathbf{r}) - f(\mathbf{r}_i - \mathbf{r})] d\mathbf{r}, \end{aligned} \quad (\text{B1})$$

where the cutoff function $f(\mathbf{r})$ is the $1/r$ Coulomb interaction defined within the ‘‘nearest image’’ convention, which corresponds to reducing the vector \mathbf{r} into the Wigner-Seitz (WS) cell of the simulation cell, v_E is the Ewald potential, and n is the electronic charge density from the many-electron wave function Ψ . The electron-electron contribution to the total energy is the expectation value of $\hat{H}_{e-e}^{\text{exact}}$ with Ψ , minus a double counting term,

$$\begin{aligned} E_{e-e}^{\text{exact}} &= \langle \Psi | \hat{H}_{e-e}^{\text{exact}} | \Psi \rangle - \frac{1}{2} \int_{\text{WS}} n(\mathbf{r}) n(\mathbf{r}') \\ &\quad \times [v_E(\mathbf{r} - \mathbf{r}') - f(\mathbf{r} - \mathbf{r}')] d\mathbf{r} d\mathbf{r}'. \end{aligned} \quad (\text{B2})$$

It is straightforward to show that with this expression the Hartree energy is evaluated with the Ewald interaction while the exchange-correlation energy is evaluated with the cutoff interaction.

In a DMC calculation we require the local energy at every time step, but the DMC charge density, n , is only known at the end of the run. Also, it is rather inconvenient to have to subtract the double counting term. We therefore define an approximate MPC Hamiltonian as

$$\begin{aligned} \hat{H}_{e-e} &= \sum_{i>j} f(\mathbf{r}_i - \mathbf{r}_j) + \sum_i \int_{\text{WS}} n_A(\mathbf{r}) \\ &\quad \times [v_E(\mathbf{r}_i - \mathbf{r}) - f(\mathbf{r}_i - \mathbf{r})] d\mathbf{r} - \frac{1}{2} \int n_A(\mathbf{r}) n_A(\mathbf{r}') \\ &\quad \times [v_E(\mathbf{r} - \mathbf{r}') - f(\mathbf{r} - \mathbf{r}')] d\mathbf{r} d\mathbf{r}', \end{aligned} \quad (\text{B3})$$

where n_A is an approximate charge density obtained either from an independent particle calculation or a VMC calculation. Because of the presence of the third term on the right hand side, which is a constant, there is no double counting and the interaction energy is simply $E_{e-e} = \langle \Psi | \hat{H}_{e-e} | \Psi \rangle$. It is straightforward to show that

$$\begin{aligned} E_{e-e} &= E_{e-e}^{\text{exact}} - \frac{1}{2} \int_{\text{WS}} [n(\mathbf{r}) - n_A(\mathbf{r})][n(\mathbf{r}') - n_A(\mathbf{r}')] \\ &\quad \times [v_E(\mathbf{r} - \mathbf{r}') - f(\mathbf{r} - \mathbf{r}')] d\mathbf{r} d\mathbf{r}'. \end{aligned} \quad (\text{B4})$$

The error due to using the approximate charge density n_A is second order in $(n - n_A)$ and the operator $(v_E - f)$ becomes small for large simulation cell sizes. For any reasonable

ap proximation to the charge density and simulation cell size the error term is usually extremely small and we neglect it, although it could be calculated at the end of the simulation.

In our implementation the first term in Eq. (B3) is evalu-

ated in real space and the second term in Fourier space. The third term is a constant which is evaluated in Fourier space at the start of the calculation. We use the MPC Hamiltonian of Eq. (B3) in both VMC and DMC calculations.

- ¹W.M.C. Foulkes, L. Mitas, R.J. Needs, and G. Rajagopal, *Rev. Mod. Phys.* **73**, 33 (2001).
- ²E. Jensen and E.W. Plummer, *Phys. Rev. Lett.* **55**, 1912 (1985).
- ³I. Lyo and E.W. Plummer, *Phys. Rev. Lett.* **60**, 1558 (1988).
- ⁴H. Yasuhara, S. Yoshinaga, and M. Higuchi, *Phys. Rev. Lett.* **83**, 3250 (1999); M. Higuchi, S. Yoshinaga, and H. Yasuhara, *J. Phys. Soc. Jpn.* **68**, 3473 (1999); T. Ishihara, H. Yamagami, and H. Yasuhara, *ibid.* **70**, 3613 (2001).
- ⁵J.B. Anderson, *J. Chem. Phys.* **65**, 4121 (1976).
- ⁶J.W. Moskowitz, K.E. Schmidt, M.A. Lee, and M.H. Kalos, *J. Chem. Phys.* **77**, 349 (1982).
- ⁷P.J. Reynolds, D.M. Ceperley, B.J. Alder, and W.A. Lester, Jr., *J. Chem. Phys.* **77**, 5593 (1982).
- ⁸W.M.C. Foulkes, R.Q. Hood, and R.J. Needs, *Phys. Rev. B* **60**, 4558 (1999).
- ⁹V. R. Saunders, R. Dovesi, C. Roetti, M. Causà, N. M. Harrison, R. Orlando, and C. M. Zicovich-Wilson, *CRYSTAL98 User's Manual* (University of Torino, Torino, 1998).
- ¹⁰J.P. Perdew, K. Burke, and M. Ernzerhof, *Phys. Rev. Lett.* **77**, 3865 (1996).
- ¹¹Y. Lee and R.J. Needs, *Phys. Rev. B* **67**, 035121 (2003).
- ¹²Y. Lee, P.R.C. Kent, M.D. Towler, R.J. Needs, and G. Rajagopal, *Phys. Rev. B* **62**, 13347 (2000).
- ¹³M.M. Hurley and P.A. Christiansen, *J. Chem. Phys.* **86**, 1069 (1987); B.L. Hammond, P.J. Reynolds, and W.A. Lester, Jr., *ibid.* **87**, 1130 (1987); L. Mitas, E.L. Shirley, and D.M. Ceperley, *ibid.* **95**, 3467 (1991).
- ¹⁴R. J. Needs, M. D. Towler, N. D. Drummond, P. R. C. Kent, G. Rajagopal, and A. J. Williamson, *CASINO version 1.5 User's Manual* (University of Cambridge, Cambridge, 2002).
- ¹⁵T. Kato, *Commun. Pure Appl. Math.* **10**, 151 (1957).
- ¹⁶C.J. Umrigar, K.G. Wilson, and J.W. Wilkins, *Phys. Rev. Lett.* **60**, 1719 (1988).
- ¹⁷P.R.C. Kent, R.J. Needs, and G. Rajagopal, *Phys. Rev. B* **59**, 12 344 (1999).
- ¹⁸O. Blaschko, V. Dmitriev, G. Krexner, and P. Toledano, *Phys. Rev. B* **59**, 9095 (1999), and references therein.
- ¹⁹C.S. Barrett, *Acta Crystallogr.* **9**, 671 (1956).
- ²⁰R. Gaudoin, W.M.C. Foulkes, and G. Rajagopal, *J. Phys.: Con-*
dens. Matter **14**, 8787 (2002).
- ²¹We use Hartree atomic units ($\hbar = e^2 = m_e = 4\pi\epsilon_0 = 1$) for all equations.
- ²²W. Müller, J. Flesch, and W. Meyer, *J. Chem. Phys.* **80**, 3297 (1984).
- ²³E.L. Shirley and R.M. Martin, *Phys. Rev. B* **47**, 15413 (1993).
- ²⁴L.M. Fraser, W.M.C. Foulkes, G. Rajagopal, R.J. Needs, S.D. Kenny, and A.J. Williamson, *Phys. Rev. B* **53**, 1814 (1996).
- ²⁵A.J. Williamson, G. Rajagopal, R.J. Needs, L.M. Fraser, W.M.C. Foulkes, Y. Wang, and M.-Y. Chou, *Phys. Rev. B* **55**, R4851 (1997).
- ²⁶P.R.C. Kent, R.Q. Hood, A.J. Williamson, R.J. Needs, W.M.C. Foulkes, and G. Rajagopal, *Phys. Rev. B* **59**, 1917 (1999).
- ²⁷R.Q. Hood, M.-Y. Chou, A.J. Williamson, G. Rajagopal, R.J. Needs, and W.M.C. Foulkes, *Phys. Rev. Lett.* **78**, 3350 (1997).
- ²⁸R.Q. Hood, M.-Y. Chou, A.J. Williamson, G. Rajagopal, and R.J. Needs, *Phys. Rev. B* **57**, 8972 (1998).
- ²⁹*CRC Handbook of Chemistry and Physics*, 76th ed., edited by D. R. Lide (CRC, New York, 1996), pp. 10–207.
- ³⁰J. de Launay, in *Solid State Physics*, Vol. 2, edited by F. Seitz and D. Turnbull (Academic, New York, 1956), pp. 232 and 233, Tables I and II.
- ³¹J.E. Jaffe, Z. Lin, and A.C. Hess, *Phys. Rev. B* **57**, 11 834 (1998).
- ³²K. A. Gschneidner, Jr., in *Solid State Physics*, edited by F. Seitz and D. Turnbull (Academic, New York, 1964), Vol. 16, p. 344.
- ³³R. J. Needs, A. R. Porter, and M. D. Towler, in *Recent Advances in Quantum Monte Carlo Methods, Part II*, edited by W. A. Lester, Jr., S. M. Rothstein, and S. Tanaka (World Scientific, Singapore, 2002), p. 143.
- ³⁴Y. Takada, in *Tatai-mondai* (Asakura Shoten, Tokyo, 1999).
- ³⁵Y. Takada, *Phys. Rev. Lett.* **87**, 226402 (2001).
- ³⁶W. Ku, A.G. Eguluz, and E.W. Plummer, *Phys. Rev. Lett.* **85**, 2410 (2000); H. Yasuhara, S. Yoshinaga, and M. Higuchi, *ibid.* **85**, 2411 (2000).
- ³⁷A.J. Williamson, R.Q. Hood, R.J. Needs, and G. Rajagopal, *Phys. Rev. B* **57**, 12 140 (1998).
- ³⁸M.D. Towler, R.Q. Hood, and R.J. Needs, *Phys. Rev. B* **62**, 2330 (2000).
- ³⁹W.-K. Leung, Ph.D. thesis, University of Cambridge, 2001.